Journal of Magnetism and Magnetic Materials 322 (2010) 242–246

Contents lists available at ScienceDirect

Journal of Magnetism and Magnetic Materials

journal homepage: www.elsevier.com/locate/jmmm

Crossover of critical behavior in $La_{0.7}Ca_{0.3}Mn_{1-x}Ti_xO_3$

Xuebin Zhu [a], Yuping Sun [a], Xuan Luo [a], Hechang Lei [a], Bosen Wang [a], Wenhai Song [a], Zhaorong Yang [a], Jianming Dai [a], Dongqi Shi [b], Shixue Dou [b]

[a] Key Laboratory of Materials Physics, Institute of Solid State Physics, Chinese Academy of Sciences, Hefei 230031, People's Republic of China
[b] Institute for Superconducting and Electronic Materials, University of Wollongong, NSW 2522, Australia

ARTICLE INFO

Article history:
Received 4 April 2009
Received in revised form
21 August 2009
Available online 6 September 2009

PACS:
75.47Lx
64.60.f
75.40Cx

Keywords:
Colossal magnetoresistance
Critical behavior

ABSTRACT

Critical behavior of Ti-doped $La_{0.7}Ca_{0.3}MnO_3$ ceramics are studied using magnetization methods. The results show that the paramagnetic–ferromagnetic transition is first order for the undoped sample, then for low-doping samples the mean-field model is suitable, and finally a 3D Heisenberg model is satisfied for higher doping samples. These findings demonstrate that the critical behavior of the magnetic transition for manganites is sensitive to Mn-site doping.

1. Introduction

In the last decades, intensive research has been focused on the perovskite colossal magnetoresistance (CMR) manganites due to their interesting phenomena [1]. It has been recognized that the interesting properties are fundamentally originated from the double exchange (DE) between Mn^{3+}–O–Mn^{4+} [2]. Therefore, it is desired to directly study the effects of Mn-site doping. $La_{0.7}Ca_{0.3}MnO_3$ is a typical material with narrow band, and its paramagnetism–ferromagnetism (PM–FM) transition is a first order [3]. Although lots of works have been contributed to study the Mn-site doping effects, the critical exponents as very important parameters for magnetic transition are less available for the Mn-site doping. Recently, it is enlightened to observe that 10 at%-Ga substitution of Mn^{3+} ions in $La_{0.67}Ca_{0.33}MnO_3$ can turn the first order of PM–FM transition into a second one, and the obtained critical exponents are close to the values predicted by 3D Heisenberg model [4]. As for lower doping level there are no reports. It is reasonable to ask whether the first-order transition is directly turned into a second order with exponents close to 3D Heisenberg model, or other models are suitable for the lower doping conditions.

In this study, we choose $La_{0.7}Ca_{0.3}Mn_{1-x}Ti_xO_3$ ceramics to study the critical exponents. The reasons are as follows: first, it has been recognized that Ti^{4+} will substitute for Mn^{4+} ions, which is different from Ga^{3+} doping condition [5,6]. Second, it has been reported that above a critical doping level, the fundamental properties, including disappearance of insulator–metal transition and appearance of spin glass, will be obviously changed even the doping content is changed slightly. Third, it has been widely recognized that decrease in rate of Curie temperature due to Ti doping is very sharp at low Ti content, then for higher Ti content it flattens [7]. Moreover, recently Nam et al. [8,9] found that in $La_{0.7}Ca_{0.3}Mn_{1-x}Ti_xO_3$ antiferromagnetic superexchange between Mn ions is significant according to a molecular-field approximation, and also the non-equilibrium dynamic behaviors are observed in $La_{0.7}Ca_{0.3}Mn_{0.925}Ti_{0.075}O_3$. We desire that the study of the critical exponents for $La_{0.7}Ca_{0.3}Mn_{1-x}Ti_xO_3$ can provide some useful information about these interesting phenomena. Our results show that at low doping level the critical exponents are close to the parameters predicted by the mean-field theory, however, at higher doping level the critical exponents are satisfied with the 3D Heisenberg model.

2. Experimental procedures

Polycrystalline $La_{0.7}Ca_{0.3}Mn_{1-x}Ti_xO_3$ (x=0, 0.03, 0.05, 0.07 and 0.1) samples were prepared using solid state reaction. It was observed that all samples are single phase and the lattice parameters derived by the Rietveld refinement increased with Ti content, which was attributed to larger Ti^{4+} ions substitution of smaller Mn^{4+} ions. The magnetic measurements were carried out

E-mail address: xbzhu@issp.ac.cn (X. Zhu).

0304-8853/$ - see front matter © 2009 Elsevier B.V. All rights reserved.
doi:10.1016/j.jmmm.2009.09.005

with magnetic property measurement system (MPMS, Quantum-design). For the measurement of magnetic hysteresis loop, M–H, before each run, samples were heated above their Curie temperatures (T_c) and cooled to the measuring temperature under zero field in order to ensure a perfect demagnetization of the samples.

3. Results and discussion

The Arrott plot, M^2 vs. H/M, obtained from the isothermal M–H results at $1.05T_c$, shows that the slope is negative for the undoped sample indicating the first-order PM–FM transition as previously reported [3]. Whereas, for all doped samples the slope is positive indicating the second-order PM–FM transition [10]. Moreover, it is also observed that T_c decreases linearly at a rate 24 K/Ti as Ti ≤ 5 at%, then, the decreasing rate is flattened to 4 K/Ti with further Ti doping, which is also similar to previous reports. It is thought that the foresaid phenomena induced by Ti doping should be manifested in the critical behavior, and the critical exponents can provide useful information.

Since critical exponents are not defined for the first-order transition due to a field-dependent phase boundary of $T_c(H)$ [3], we will only focus on critical behavior of the doped samples. The second-order magnetic phase transition near the Curie point is characterized by a set of critical exponents, β (associated with the spontaneous magnetization), γ (relevant to the initial magnetic susceptibility) and δ (associated with the critical magnetization isotherm). The mathematical definitions of the exponents from magnetization measurements are given below [11,12]

$$M_s(T) = M_0(-\varepsilon)^{\beta}, \varepsilon < 0,\ T < T_c, \tag{1}$$

$$\chi_0^{-1}(T) = (h_0/M_0)\varepsilon^{\gamma}, \varepsilon > 0,\ T > T_c, \tag{2}$$

$$M = DH^{1/\delta}, \varepsilon = 0,\ T = T_c, \tag{3}$$

where $\varepsilon=(T-T_c)/T_c$ and M_0, h_0/M_0 and D are the critical amplitudes.

Additionally, near the critical temperature of a second-order transition, the free energy G can be expressed in terms of the order parameter M in the following form:

$$G(T,M) = G_0 + aM^2 + bM^4 - MH, \tag{4}$$

where the coefficients a and b are temperature-dependent parameters. For the condition of equilibrium, i.e., energy minimization, $\partial G/\partial M = 0$, the magnetic equation of state is obtained as

$$H/M = 2a + 4bM^2. \tag{5}$$

Fig. 1(a) and (b) is the M–H and Arrott plot of $La_{0.7}Ca_{0.3}Mn_{0.95}Ti_{0.05}O_3$. It is observed that the line below T_c (~138 K) is not linear, indicating the exponents with $\beta=0.5$ and $\gamma=1$ are not satisfied.

Using a polynomial fit as shown in Eq. (5), and extrapolating the data for $T < T_c$ give the reliable values of $M_s(T,0)$ [13]. For the extrapolation, the M^2 vs. H/M data are fitted with fourth-order polynomial function from $H=0.3$ to 4.5 T, which was then extrapolated to $H=0$ to obtain the values of $M_s(T,0)$. Above T_c, the curves can be extended smoothly into the H/M axis to yield the reliable value of $\chi_0^{-1}(T,0)$. The obtained $M_s(T,0)$ and $\chi_0^{-1}(T,0)$ are shown in Fig. 1(c). The power law fittings of $M_s(T,0)$ vs. T and $\chi_0^{-1}(T,0)$ vs. T according to Eqs. (1) and (2), respectively, give the critical exponents of $\beta=0.603\pm0.03$ with $T_c=136.16\pm0.03$ K and $\gamma=1.20\pm0.01$ with $T_c=136.37\pm0.06$ K. The exponents were also obtained using Kouvel–Fisher (KF) method in order to obtain more precise exponents [14]

$$M_s(T)[dM_s(T)/dT]^{-1} = (T - T_c)/\beta, \tag{6}$$

$$\chi_0^{-1}(T)[d\chi_0^{-1}(T)/dT]^{-1} = (T - T_c)/\gamma. \tag{7}$$

According to these equations, using the obtained $M_s(T,0)$ vs. T and $\chi_0^{-1}(T,0)$ from Fig. 1, the plotting of $M_s(T)[dM_s(T)/dT]^{-1}$ and $\chi_0^{-1}(T)[d\chi_0^{-1}(T)/dT]^{-1}$, against temperature yields straight lines with slope $1/\beta$ and $1/\gamma$, respectively, and the intercepts on the T axes are equal to T_c. The linear fit to the plots following the KF method gives $\beta=0.601\pm0.02$ with $T_c=136.10\pm0.17$ K and $\gamma=1.171\pm0.01$ with $T_c=136.50\pm0.07$ K, as shown in Fig. 1(d). The high-field region of the data from critical isotherm is fitted by a straight line with slope $1/\delta$. This gives the value of δ as 3.11 ± 0.012. The three exponents derived from static scaling analysis are related by the Widom scaling relation [15]

$$\delta = (1 + \gamma/\beta). \tag{8}$$

Using this scaling relation and estimated values of β and γ from KF method, we obtain $\delta=2.95\pm0.01$, which is close to the estimated δ from the critical isotherms at T_c as shown in Fig. 1(e). Thus, the critical exponents obtained in this study obey the Widom scaling relation, implying that the obtained β and γ values are reliable.

Next, we compare our data with the prediction of the scaling theory. In the critical region, the magnetic equation of state is given by

$$M_s(H,\varepsilon) = |\varepsilon|^{\beta} f_{\pm}(H/|\varepsilon|^{\beta+\gamma}), \tag{9}$$

where f_+ for $T > T_c$ and f_- for $T < T_c$ are regular analytical functions. Eq. (9) implies that the $M_s(H,\varepsilon)$ as a function of $H/|\varepsilon|^{\beta+\gamma}$ produces two universal curves: one for temperatures below T_c and the other for temperatures above T_c. Using the values of β and γ obtained by the KF method, the scaled data are plotted in Fig. 1(f). All the points fall on two curves, one for $T > T_c$ and the other for $T < T_c$. This suggests that the values of the exponents and T_c are reasonably accurate.

As for the highest doping sample in this study, $La_{0.7}Ca_{0.3}Mn_{0.9}Ti_{0.1}O_3$, the M–H result is shown in Fig. 2(a). Using the same treating procedure for the sample $La_{0.7}Ca_{0.3}Mn_{0.95}Ti_{0.05}O_3$, the $M_s(T,0)$ and $\chi_0^{-1}(T,0)$ for the sample $La_{0.7}Ca_{0.3}Mn_{0.9}Ti_{0.1}O_3$ can be obtained, and the results are shown in Fig. 2(b). By fitting, the obtained critical exponents are $\beta=0.388\pm0.001$ with $T_c=90.72\pm0.15$ K and $\gamma=1.482\pm0.09$ with $T_c=89.84\pm0.78$ K. Fig. 2(c) shows is the results derived by KF method, and β is 0.389 ± 0.02 with $T_c=89.65\pm0.43$ K and γ is 1.403 ± 0.03 with $T_c=90.59\pm0.27$ K. The δ values obtained from Widom method and critical isotherms as shown in Fig. 2(d) at T_c are 4.278 and 4.427, respectively. Also, for this sample, the scaled data plotted in Fig. 2(e) gives two curves, one for $T > T_c$ and another for $T < T_c$. This suggests that the values of the exponents and T_c are reasonably accurate. The obtained critical exponents suggest that the sample $La_{0.7}Ca_{0.3}Mn_{0.9}Ti_{0.1}O_3$ can be treated as 3D Heisenberg-like isotropic magnet.

Table 1 shows the relative critical exponents for our experiment as well as various theoretical models and some relative manganites including Ca-doped and Mn-site doping CMR manganites. It can be seen that with varying Ca content, the critical behavior can be changed. Also, the substitution of Sr for Ca will turn the first-order PM–FM transition into a second order when the Sr content is higher than a critical value. For the Mn-site doping condition, only high Ga content (10%at) is studied and the exponents are satisfied with 3D Heisenberg model.

From our experiment, it is observed that for the undoped sample, the PM–FM phase transition is a first order, which is same as previous reports, and then for low Ti-doping level condition the

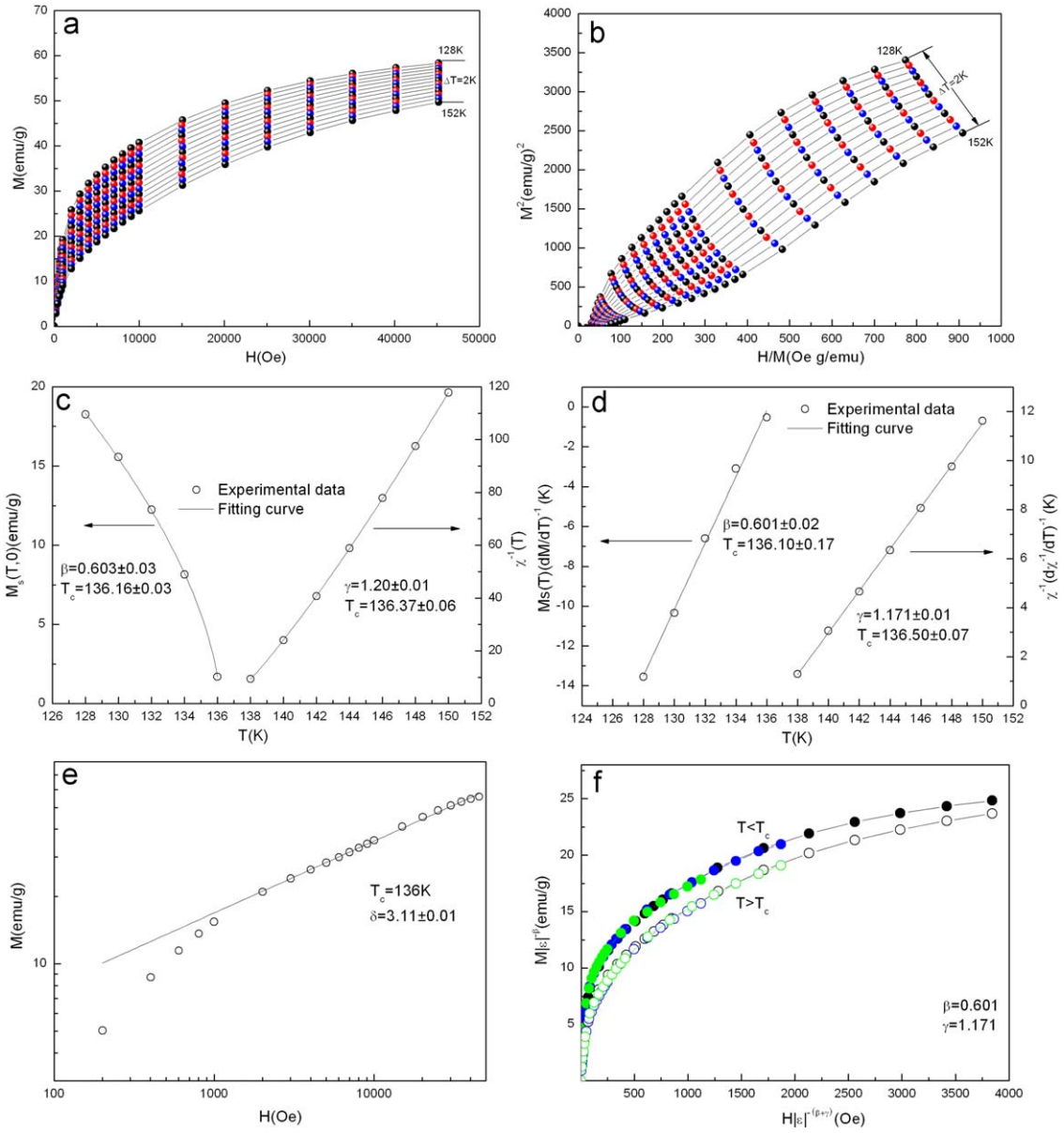

Fig. 1. Results for $La_{0.7}Ca_{0.3}Mn_{0.95}Ti_{0.05}O_3$. (a) *M–H*, (b) Arrott plot, (c) $M_s(T,0)$ and $\chi_0^{-1}(T,0)$, (d) Kouvel–Fisher plots, (e) critical isotherms and (f) scaling plots.

critical exponents are close to values predicated by the mean-field theory, and finally for higher Ti-doping level condition the model of the 3D Heisenberg-like isotropic magnet is suitable.

For the low-doping sample $La_{0.7}Ca_{0.3}Mn_{0.95}Ti_{0.05}O_3$, the critical exponents close to the values predicted by the mean-field theory as well as the appearance of insulator–metal transition (IMT, the transition temperature of 139 K as shown in Fig. 3(a)) suggest that at low doping level the sample behaves like long-range exchange interaction. The exchange interaction for this long-range FM order system can be calculated as $J(r)\sim r^{-d-\nu}$, where d is spatial dimension, ν is $1/\sigma$ (σ is the range of interaction) and $J(r)\sim 1/r^{-4.5}$ [20]. Since Ti^{4+} does not participate in DE it blocks all the conduction paths at the Ti-occupied sites. Additionally, the appearance of IMT indicates that the long-range FM order is not blocked completely. For the higher doping level sample, $La_{0.7}Ca_{0.3}Mn_{0.9}Ti_{0.1}O_3$, the critical exponents are close to the values predicted by the 3D Heisenberg model, and there is no IMT as shown in Fig. 3(b). The exchange interaction for the 3D Heisenberg-like isotropic magnet can be manifested by $J(r)\sim r^{d+\sigma}$, which decreases with the distance r faster than r^{-5}. The reduced critical amplitudes indicate the formation of spin polaron, and the cluster size is of the range about 2–3 Mn ions [21]. The formation of spin polaron will localize the e_g electrons to hop within the size of 2–3 Mn ions. The ferromagnetic spin polaron is separated by insulating non-FM boundaries, where the Ti^{4+} ions occupy the Mn^{4+} sites resulting in the depression of DE, which will induce the antiferromagnetism.

In order to further check up the magnetic properties induced by Ti-doping effects, we also measured the *M–T* under zero field and with applied field $H=100$ Oe, and the results are shown in Fig. 3(b). It can be clearly observed that the undoped and the low Ti-doping sample $La_{0.7}Ca_{0.3}Mn_{0.95}Ti_{0.05}O_3$ show the characteristics of long-range interactions; however, for the higher Ti-doping sample, $La_{0.7}Ca_{0.3}Mn_{0.9}Ti_{0.1}O_3$, it gives the evidence of spin-glass characteristics indicating short-range interactions [22]. The *M–T* results further prove that the critical behaviors for the low-doping

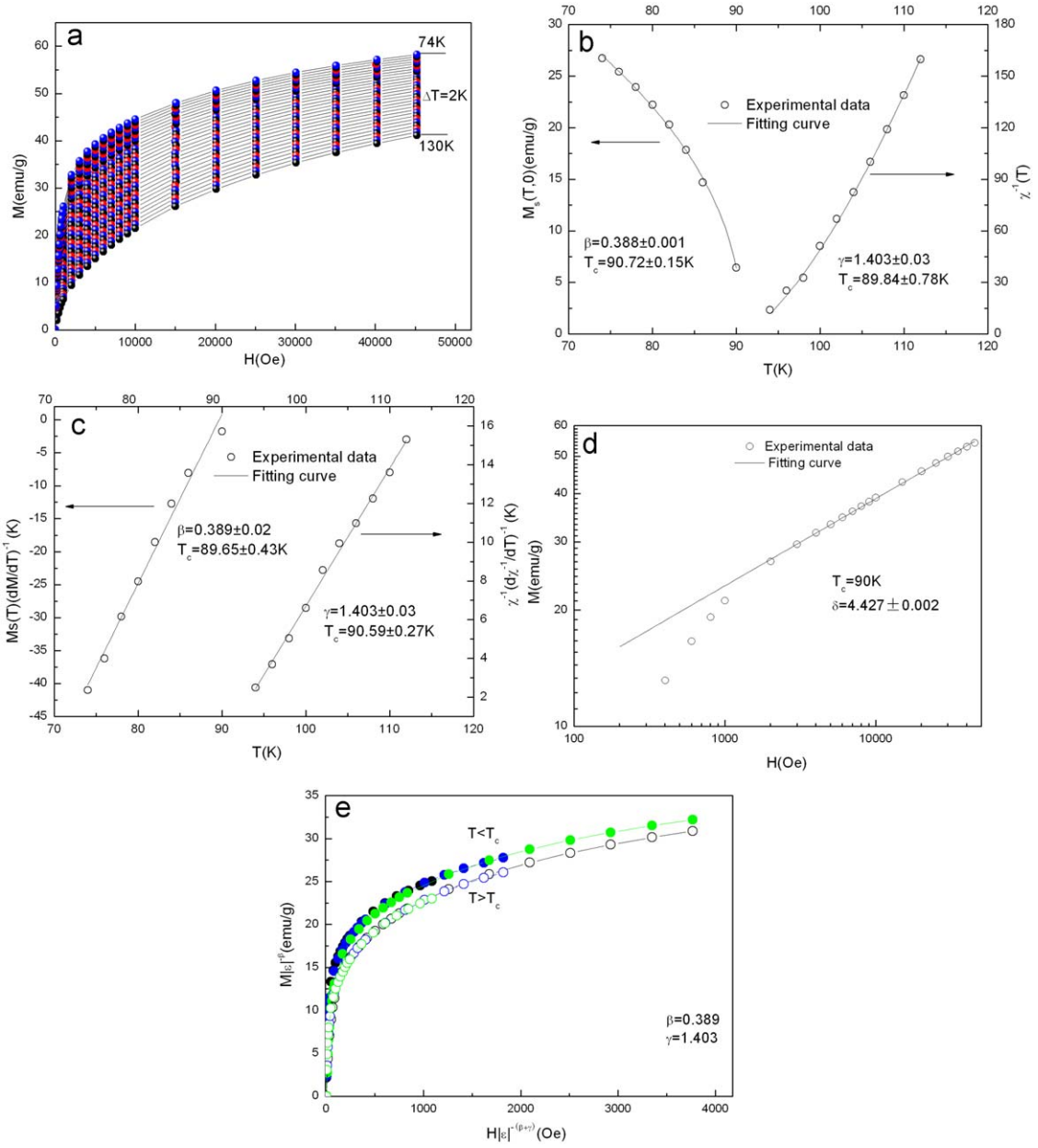

Fig. 2. Results for $La_{0.7}Ca_{0.3}Mn_{0.9}Ti_{0.1}O_3$. (a) *M–H*, (b) $M_s(T,0)$ and $\chi_0^{-1}(T,0)$, (c) Kouvel–Fisher plots, (d) critical isotherms and (e) scaling plots.

Table 1
Comparison of critical exponents for $La_{0.7}Ca_{0.3}Mn_{1-x}Ti_xO_3$ ceramics with various theory models, the Ca-doped manganites and Mn-site doping manganites ceramics reported in the literature.

Materials	β	γ	δ	Refs.
$La_{0.7}Ca_{0.3}MnO_3$	First-order transition			
$La_{0.7}Ca_{0.3}Mn_{0.95}Ti_{0.05}O_3$	0.601 ± 0.02	1.171 ± 0.01	2.95 ± 0.01	This work
$La_{0.7}Ca_{0.3}Mn_{0.93}Ti_{0.07}O_3$	0.403 ± 0.08	1.321 ± 0.01	4.28 ± 0.08	This work
$La_{0.7}Ca_{0.3}Mn_{0.9}Ti_{0.1}O_3$	0.389 ± 0.02	1.403 ± 0.03	4.40 ± 0.03	This work
Mean-field theory	0.5	1	3.0	[12]
3D Heisenberg theory	0.365 ± 0.003	1.336 ± 0.004	4.8 ± 0.04	[12]
3D Ising theory	0.325 ± 0.02	1.241 ± 0.002	4.82 ± 0.02	[12]
Tricritical mean-field theory	0.25	1	5	[3]
$La_{0.6}Ca_{0.4}MnO_3$	0.25 ± 0.03	1.03 ± 0.05	5 ± 0.8	[3]
$La_{0.7}Ca_{0.3}MnO_3$	0.14 ± 0.02	0.81 ± 0.03	1.22 ± 0.02	[16]
$La_{0.67}Ca_{0.33}MnO_3$ (15 nm)	0.47 ± 0.01	1.06 ± 0.03	3.1 ± 0.13	[17]
$La_{0.67}Ca_{0.33}Mn_{0.9}Ga_{0.1}O_3$	0.387 ± 0.06	1.362 ± 0.002	4.60 ± 0.03	[4]
$LaMn_{1-x}Ti_xO_3$	$0.359 \le \beta \le 0.378$	$1.24 \le \gamma \le 1.29$	$4.11 \le \delta \le 4.21$	[18]
$La_{2/3}(Ca_{0.95}Sr_{0.05})_{1/3}MnO_3$	First-order transition			[19]
$La_{2/3}(Ca_{0.85}Sr_{0.15})_{1/3}MnO_3$	Second-order transition without giving exponents			[19]

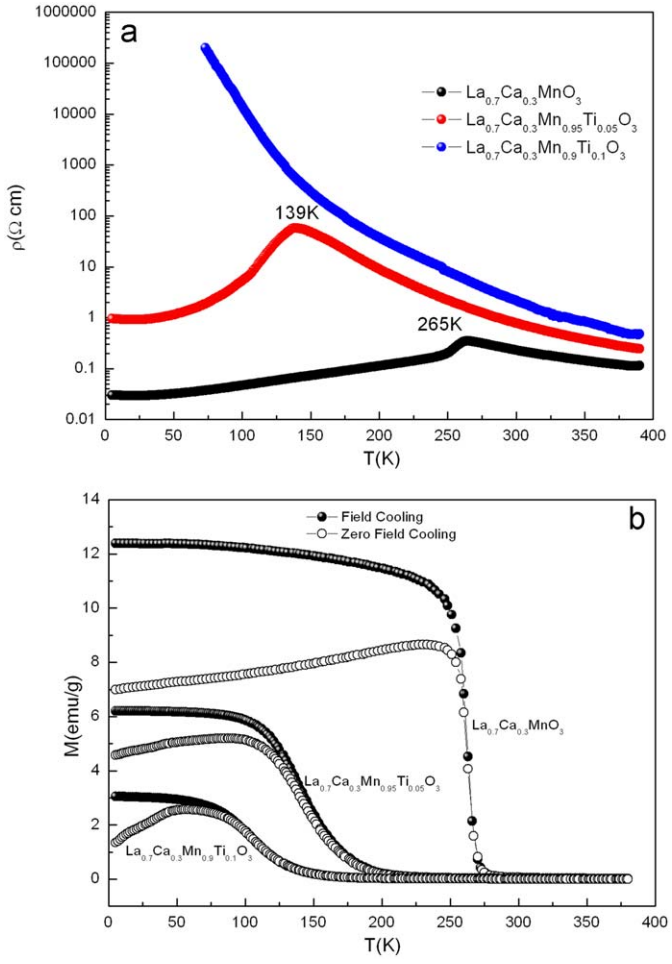

Fig. 3. Temperature dependence of resistivity and magnetization for three typical samples. (a) ρ–T; (b) M–T.

and high-doping samples should be classified into long-range and short-range exchange interactions as predicted by the mean-field and the 3D Heisenberg model, respectively.

4. Conclusion

Critical behaviors of Ti-doped $La_{0.7}Ca_{0.3}MnO_3$ ceramics were studied using the magnetization method. The results showed that for the undoped sample it was the characteristic of first-order paramagnetism–ferromagnetism transition; for the low Ti-content doping condition, the mean-field theory was suitable indicating long-range interactions; with further Ti content, the critical exponents of 3D Heisenberg model are satisfied indicating the short-range interactions with concomitance of spin glass. The crossover of critical behaviors can be applied to explain some interesting phenomena due to Mn-sites doping effects.

Acknowledgement

This work was supported by the National Key Basic Research under Contract no. 2007CB925001 and 2007CB925002, the National Science Foundation of China under Contract no. 10774146, 10774147, 50672099 and 50701042 and Director's Fund of Hefei Institutes of Physical Science, Chinese Academy of Sciences.

References

[1] M.B. Salamon, M. Jaime, Rev. Mod. Phys. 73 (2001) 583;
J.M.D. Coey, M. Viret, S. Von Molnar, Adv. Phys. 48 (1999) 167;
E. Dagotto, New J. Phys. 6 (2005) 67;
Y. Tokura, Y. Tomioka, J. Magn. Magn. Mater. 200 (1999) 1.
[2] C. Zener, Phys. Rev. 82 (1951) 403.
[3] D. Kim, B. Revaz, B.L. Zink, F. Hellman, J.J. Rhyne, J.F. Mitchell, Phys. Rev. Lett. 89 (2002) 227202.
[4] S. Rößler, U.K. Rößler, K. Nenkov, D. Eckert, S.M. Yusrf, K. Dörr, K.H. Müller, Phys. Rev. B 70 (2004) 104417.
[5] X.M. Liu, X.J. Xu, Y.H. Zhang, Phys. Rev. B 62 (2000) 15112.
[6] D. Cao, F. Brides, M. Andeson, A.P. Ramirez, M. Olapinski, M.A. Subramanian, C.H. Booth, G.H. Kwei, Phys. Rev. B 64 (2001) 184409.
[7] R.W. Li, Z.H. Wang, X. Chen, J.R. Sun, B.G. Shen, C.H. Yan, J. Appl. Phys. 87 (2001) 5597.
[8] D.N.H. Nam, N.V. Khien, N.V. Dai, L.V. Hong, N.X. Phuc, Phys. Rev. B 77 (2008) 214406.
[9] D.N.H. Nam, N.V. Dai, T.D. Thanh, L.T.C. Tuong, L.V. Hong, N.X. Phuc, Phys. Rev. B 77 (2008) 224420.
[10] S.K. Banerjee, Phys. Lett. 12 (1964) 16.
[11] M.E. Fisher, Rep. Prog. Phys. 30 (1967) 615.
[12] H.E. Stanley, Introduction to Phase Transitions and Critical Phenomena, Oxford University Press, London, 1971.
[13] J. Yang, Y.P. Lee, Y. Li, Phys. Rev. B 76 (2007) 054442.
[14] J.S. Kouvel, M.E. Fisher, Phys. Rev. 136 (1964) A1626.
[15] B. Widom, J. Chem. Phys. 41 (1964) 1633;
B. Widom, J. Chem. Phys. 43 (1965) 3898.
[16] H.S. Shi, J.E. Lee, Y.S. Nam, H.L. Ju, C.W. Park, Solid State Commun. 118 (2001) 377.
[17] T. Sarkar, A.K. Raychaudhuri, ArXiv (2008) 0804.3641v1.
[18] J. Yang, Y.P. Lee, Appl. Phys. Lett. 91 (2007) 142512.
[19] J. Mira, J. Rivas, F. Rivahulla, C. Vázquez-Vázquez, M.A. López-Quintela, Phys. Rev. B 60 (1999) 2998.
[20] M.E. Fisher, S.K. Ma, B.G. Nickel, Phys. Rev. Lett. 29 (1972) 917.
[21] M. Ziese, J. Phys.: Condens. Matter 13 (2001) 2919.
[22] K. Binder, A.P. Young, Rev. Mod. Phys. 58 (1986) 801.